Supporting Information

Highly efficient tandem luminescent solar concentrators based on eco-friendly copper iodide based hybrid nanoparticles and carbon dots

Jiancang Chen [a#], Haiguang Zhao [b#], Zhilin Li [a], Xiujian Zhao [a], Xiao Gong*[a]

a. State Key Laboratory of Silicate Materials for Architectures, Wuhan University of Technology, Wuhan 430070, P. R. China.

b. State Key Laboratory of Bio-Fibers and Eco-Textiles & College of Textiles & Clothing, College of Physics, Qingdao University, No. 308 Ningxia Road, Qingdao 266071, P. R. China.

* Corresponding author:

E-mail address: xgong@whut.edu.cn (X. Gong)

[#] equal contribution

Experimental and Methods

Materials. Cuprous iodide (CuI, 98%), potassium iodide (KI, ≥ 99.0%), PVP K30 (Mw ≈ 40000), sodium citrate (98%), urea (99%), ethyl acetate (99.5%), and methanol were purchased from Aladdin Reagent Co., Ltd, China. Potassium iodide (KI, 99%), PVP K88-96 (Mw ≈ 1300000), triethylenediamine (Ted, 99%), 1-bromopropane (> 99.0%), and PMMA (≥ 99.0%) were purchased from Macklin Reagent Co., Ltd, China. Barium chloride dihydrate (BaCl$_2$·2H$_2$O, ≥ 99.5%), toluene (≥ 99.5%), and acetone (≥ 99.5%) were supplied by Sinopharm Chemical Reagent Co., Ltd, China. All reagents were directly used as purchased without further purification.

Synthesis of 1-propyl-1,4-diazabicyclo[2.2.2]octan-1-ium (pr-ted). Firstly, 2.2893 g Ted was dissolved into 100 mL acetone by sonication. After dissolution and dispersion, 2.4847 g 1-bromopropane was slowly added to the mixed solution and stirred until an oily precipitate formed. After being washed with ethyl acetate and dried, the oily precipitate was collected[1].

Synthesis of Cu$_4$I$_6$(pr-ted)$_2$ pure powder. 0.1943 g CuI was dissolved in 2 mL saturated KI solution via sonication. 0.16 g pr-ted was dissolved in 2 mL absolute ethanol and added to CuI/KI solution. The white precipitate formed immediately and was collected by centrifugation[2].

Synthesis of Cu$_4$I$_6$(pr-ted)$_2$ NPs. Cu$_4$I$_6$(pr-ted)$_2$ NPs were synthesized following the previously reported procedures with modifications[2]. 10 g PVP K88-96 was dissolved in 1000 mL absolute ethanol, then the CuI/KI solution formed by dissolving 1.943 g CuI in 20 mL saturated KI solution was slowly added to PVP/ethanol solution upon stirring. Furthermore, 1.6 g pr-ted was dispersed in 20 mL absolute ethanol and added to the PVP/CuI/KI solution upon vigorous stirring. After being stirred for 12 h, colloidal nanoparticle suspension was obtained. The colloidal nanoparticle suspension was centrifuged at 4000 rpm for 5 min and the supernatant was retained. Then, Cu$_4$I$_6$(pr-ted)$_2$ NPs obtained by high-speed centrifugation (10000 rpm, 10 min) for the supernatant were washed with deionized water and ethanol, respectively, and collected.

Synthesis of CDs. CDs were synthesized via a solvothermal method following the previously published protocol with modifications[3,4]. 0.2941 g sodium citrate, 0.1201 g

urea, and 1.4656 g BaCl$_2$·2H$_2$O were added to 10 mL toluene and the mixture was sonicated for 10 min. Then the solution was transferred to a Teflon-lined autoclave (25 mL) and heated at 180 °C for 16 h. After the reaction, the reactor was removed and cooled naturally to room temperature. Subsequently, the solution was purified with a 0.22 μm filter membrane and the filtrate was dialyzed with a dialysis membrane (MWCO 1000) for 5 h. After purification, the powder of CDs was obtained by rotary evaporation.

Cu$_4$I$_6$(pr-ted)$_2$ NPs/PVP based LSCs. 10 mL Cu$_4$I$_6$(pr-ted)$_2$ NPs methanol solution containing different concentrations of Cu$_4$I$_6$(pr-ted)$_2$ NPs (75-300 mg mL^{-1}) was mixed uniformly with 5 g PVP K30 to form Cu$_4$I$_6$(pr-ted)$_2$ NPs/PVP solution. Then, the Cu$_4$I$_6$(pr-ted)$_2$ NPs/PVP solution was spin-coated twice at 2000 rpm for 60 s on glass substrates (5 × 5 × 0.2 cm^3) and dried at 50 °C for 5 h to obtain Cu$_4$I$_6$(pr-ted)$_2$ NPs/PVP based LSCs.

CDs/PMMA based LSCs. 10 mL CDs solution (toluene) was mixed with 10 mL PMMA solution (toluene) to form CDs/PMMA solution with a final concentration of CDs of 8 mg mL^{-1} and PMMA of 0.1 g mL^{-1}. The CDs/PMMA solution was then drop-cast on the surfaces of glass substrates with dimensions of 5 × 5 × 0.2 cm^3 and dried at room temperature for 24 h to form CDs/PMMA based LSCs.

Characterization. X-ray diffraction (XRD) analysis was carried out using a D8 Advance diffractometer (Bruker, Germany) with the Cu-Kα radiation (λ=0.15418 nm). The morphology of samples is characterized via transmission electron microscopy (TEM) (JEM-2100F, JEOL, Japan). The scanning electron microscope (SEM) examination of thin-film LSCs was performed using a JSM-7500F SEM (JEOL, Japan). Fourier transform infrared (FTIR) spectra of samples were measured On a Nicolet 6700 FTIR spectrometer (Thermo Electron Co., USA). X-ray photoelectron spectroscopy (XPS) was conducted on an ESCALAB 250 XI electron spectrometer (Thermo, USA). UV2600 UV–Vis spectrometer (Shimadzu Corp., Tokyo, Japan) was used for UV–Vis absorption spectra. PL spectra were recorded on a time-resolved fluorescence spectrometer (FL3-22, Jobin–Yvon, USA). Time decay measurements were carried out at room temperature using an automatic delay stage (M-ILS300LM, Newport, USA).

Absolute PLQY was acquired using a FLS980 fluorescence spectrophotometer (Edinburgh Instruments, UK). The temperature dependent PL measurements for the LSC were recorded on an Edinburgh FLS1000 instrument equipped with Oxford Instruments NanoScience (Tubney Woods, Abingdon OX13 5QX, UK).

Photovoltaic properties of single-layer LSC and tandem LSCs were measured under a simulated spectrum (AM 1.5G, 100 mW cm^{-2}) by a calibrated solar simulator (IV4112, Newport Corp., Irvine, CA, USA). $Cu_4I_6(pr\text{-}ted)_2$ NPs/PVP based LSC as the LSC top layer was stacked with CDs/PMMA based LSC as the LSC bottom layer to comprise the tandem LSCs (dimensions: $5 \times 5 \times 0.2$ cm^3). In addition, an air gap of 2 mm was introduced between the LSC top layer and the LSC bottom layer. The tandem LSCs were measured by one solar cell. A crystalline-silicon (c-Si) solar cell (Fraflor) was coupled to one edge of the tandem LSCs, and the extra portion was covered with black tape. No mirrors were used in this work. The stability of the tandem LSCs was investigated by measuring the power conversion efficiency of $Cu_4I_6(pr\text{-}ted)_2$ NPs/PVP based LSCs and CDs/PMMA based LSCs within 14 days in ambient conditions (under natural sunlight irradiation in Wuhan, China; the average daily light intensity: ~ 64 mW cm^{-2}; the average daily illumination time: ~ 10.5 hours).

Theoretical Simulation

The optical conversion efficiency of the LSCs is expressed as following based on the reported literature[5]:

$$\eta_{opt} = \eta_{Abs} \cdot \eta_{internal} \qquad \text{(Eq. 1)}$$

Where η_{Abs} is the fraction of absorbed sunlight by the LSC (Figure S7) and $\eta_{internal}$ is the internal quantum efficiency of the LSC.

η_{Abs} can be calculated as[5]:

$$\eta_{Abs} = \frac{\int_0^\infty I_{in}(\lambda)(1 - e^{-\alpha(\lambda)d})d\lambda}{\int_0^\infty I_{in}(\lambda)d\lambda} \qquad \text{(Eq. 2)}$$

In which α is the absorption coefficient calculated as $\alpha = \ln{(10)}\dfrac{A}{d}$, where d is the effective length (0.2 cm in the simulation), A is the absorption of the LSC measured by the absorption spectra, and I_{in} is the Sun irradiance.

A spectrally averaged internal efficiency ($\eta_{internal}$) over the PL emission of the QDs was calculated as[5]:

$$\eta_{internal} = \dfrac{\displaystyle\int_0^\infty \dfrac{\eta_{QY}P_{TIR}}{1 + \beta\alpha(\lambda)L_{lsc}(1 - \eta_{QY}P_{TIR})}S_{PL}(\lambda)d\lambda}{\displaystyle\int_0^\infty S_{PL}(\lambda)d\lambda}$$

(Eq. 3)

in which $S_{PL}(\lambda)$ is the normalized PL emission spectrum (Figure S7); β is a numerical value fixed to 1.4 and L_{lsc} is the length of the LSC (1-100 cm). η_{QY} is 92.2%. Assuming an isotropic emission, P_{TIR} is defined by the escape cone identified by the critical angle θ of the air/glass interface:

$$P_{TIR} = \sqrt{1 - \left(\dfrac{n_{air}}{n}\right)^2}$$

(Eq. 4)

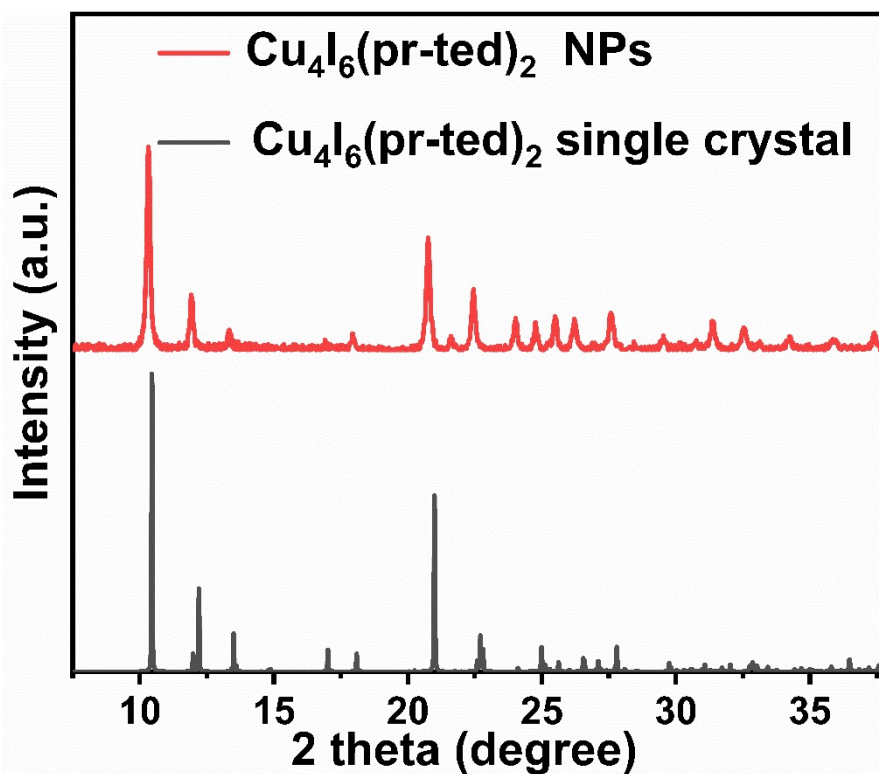Where n_{air} is 1 and n of the glass is 1.49. The calculated P_{TIR} is 0.74.

Results:

Fig. S1 XRD pattern of $Cu_4I_6(pr\text{-}ted)_2$ NPs (red) and simulated XRD pattern from $Cu_4I_6(pr\text{-}ted)_2$ single crystal (black).
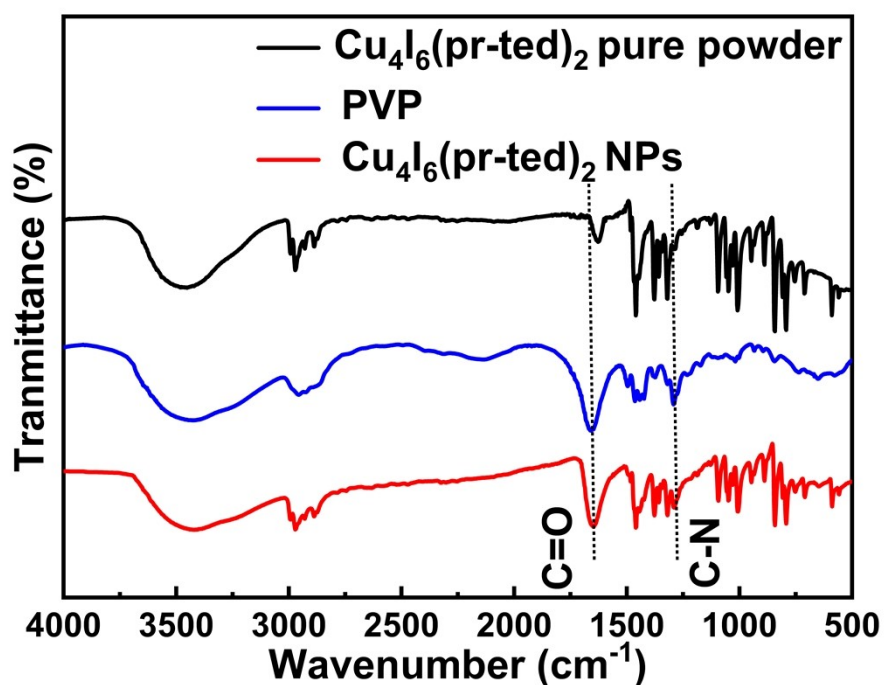

Fig. S2 FT-IR spectra of $Cu_4I_6(pr\text{-}ted)_2$ pure powder (black), PVP K88-96 (blue) and $Cu_4I_6(pr\text{-}ted)_2$ NPs (red).
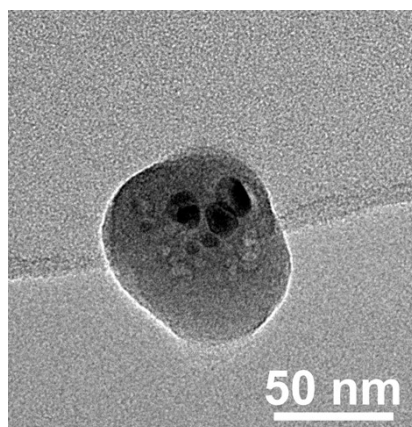
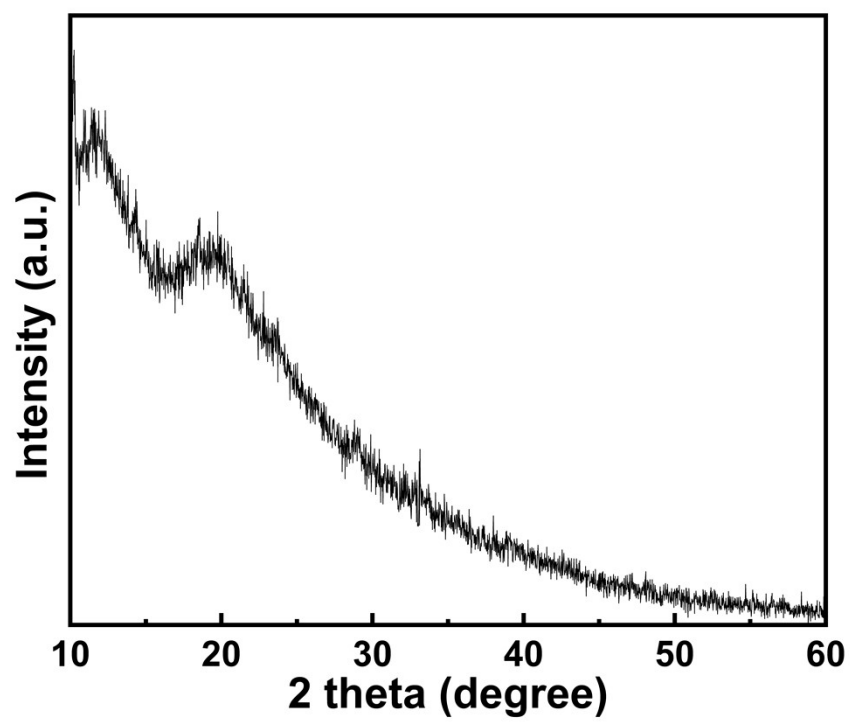**Fig. S3** TEM image of $Cu_4I_6(pr\text{-}ted)_2$ single nanoparticle.
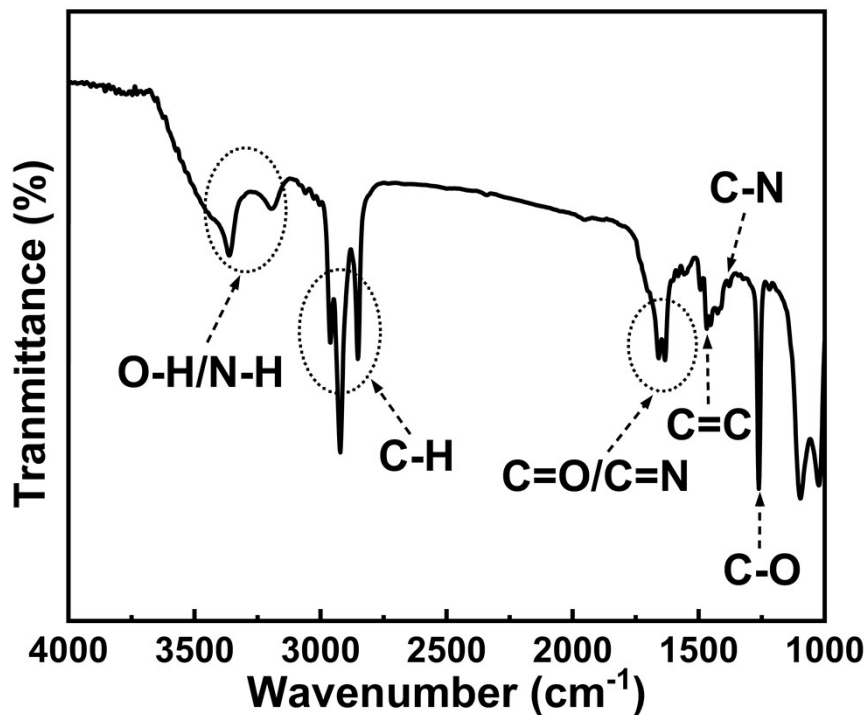

Fig. S4 XRD pattern of CDs.
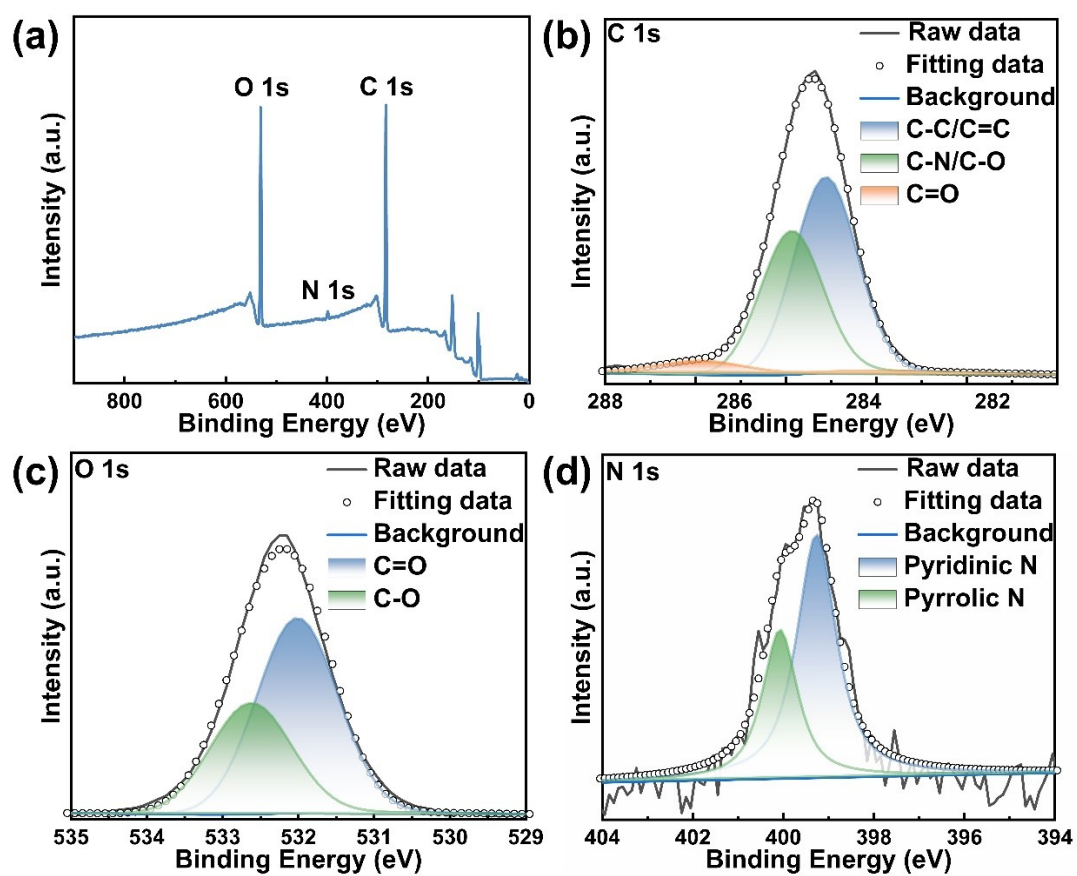
Fig. S5 FTIR spectra of CDs.

Fig. S6 XPS spectra of CDs. (a) XPS survey spectrum and (b) C1s, (c) O1s, and (d) N1s high-
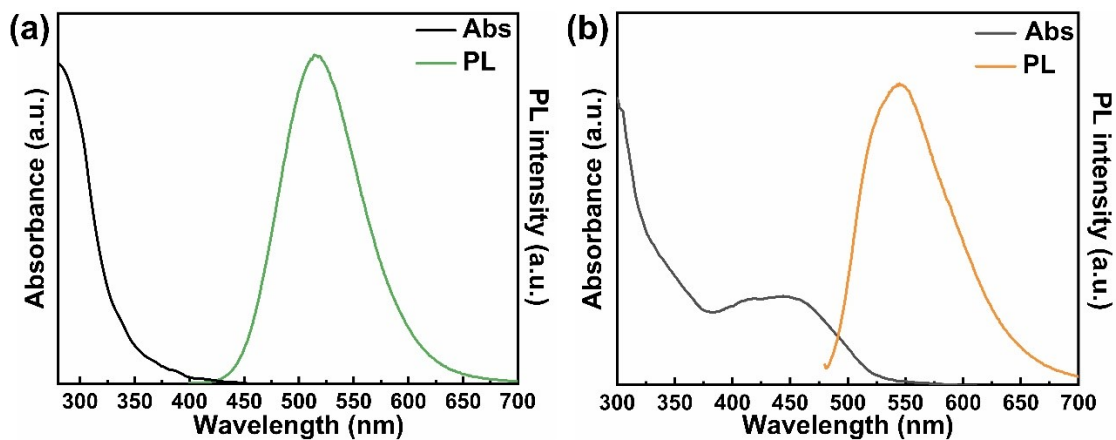
resolution XPS spectra of the CDs.

Fig. S7 Absorption and emission spectra of $Cu_4I_6(pr\text{-}ted)_2$ NPs in a PVP polymer film (a) and CDs in a PMMA polymer film (b).
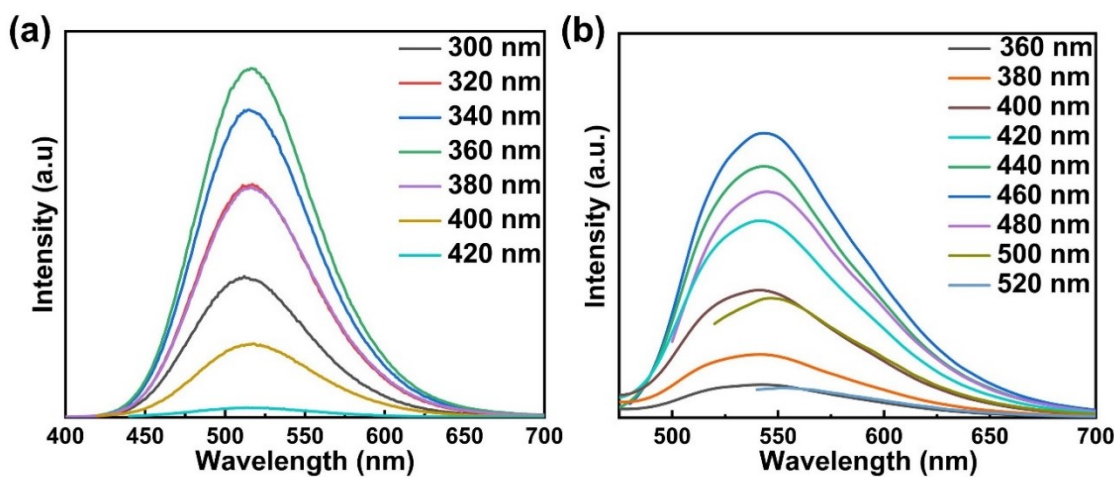

Fig. S8 The PL spectra of $Cu_4I_6(pr\text{-}ted)_2$ NPs/PVP based LSCs (a) and CDs/PMMA based LSCs (b) under different excitation wavelengths.
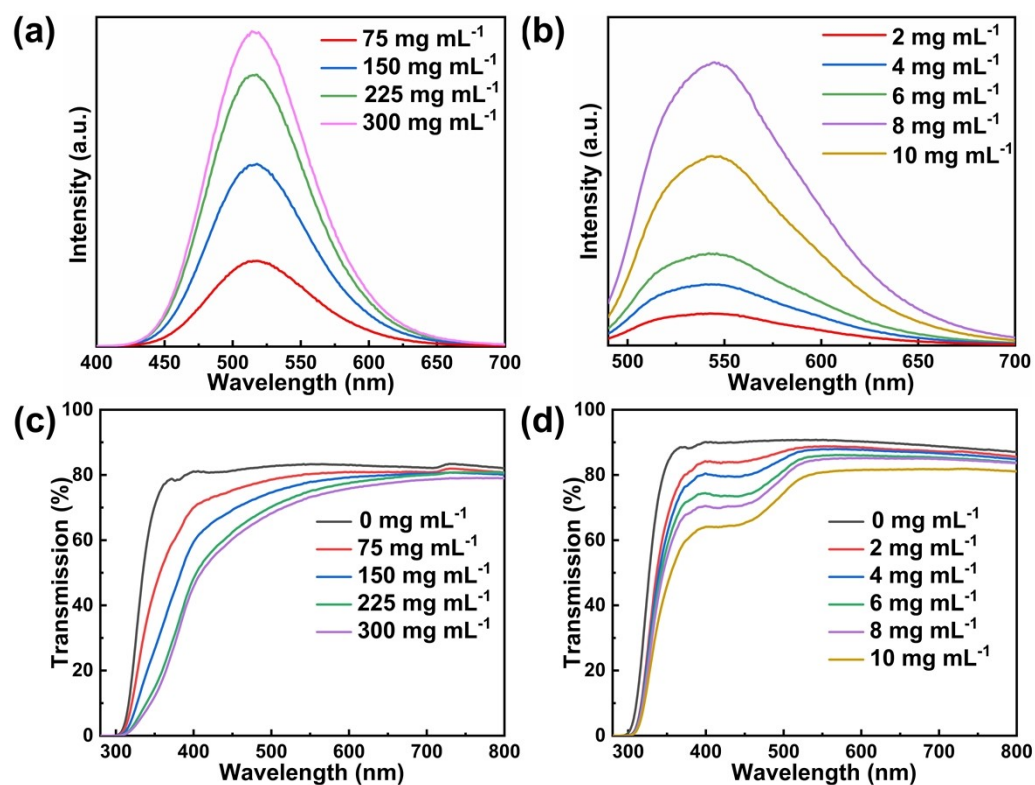
Fig. S9 PL spectra of $Cu_4I_6(pr\text{-}ted)_2$ NPs/PVP based LSCs with various concentrations of $Cu_4I_6(pr\text{-}ted)_2$ NPs (a) and CDs/PMMA based LSCs with various concentrations of CDs (b). Transmittance spectra of $Cu_4I_6(pr\text{-}ted)_2$ NPs/PVP based LSCs with various concentrations of $Cu_4I_6(pr\text{-}ted)_2$ NPs (c) and CDs/PMMA based LSCs with various concentrations of CDs (d).
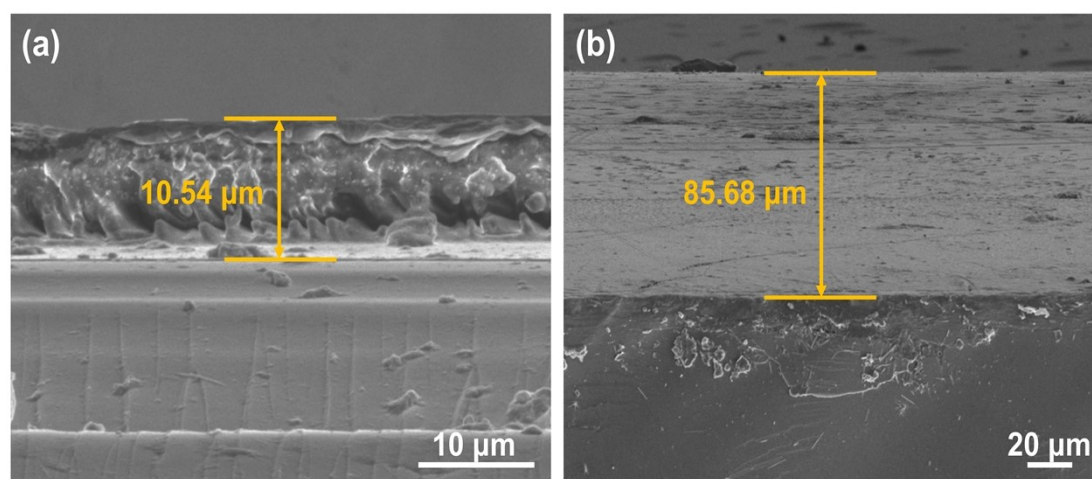

Fig. S10 SEM cross-sectional images of $Cu_4I_6(pr\text{-}ted)_2$ NPs/PVP based LSCs (a) and CDs/PMMA based LSCs (b).
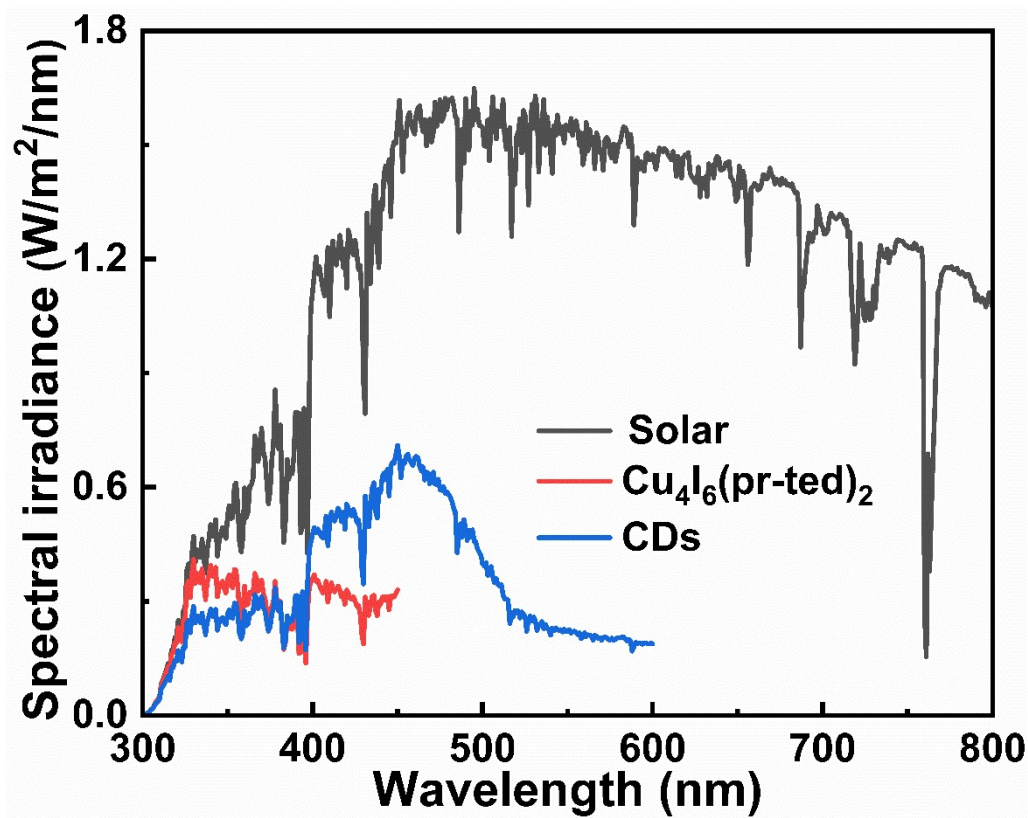
Fig. S11 Calculated solar absorption of the LSCs and solar spectrum (AM 1.5G).
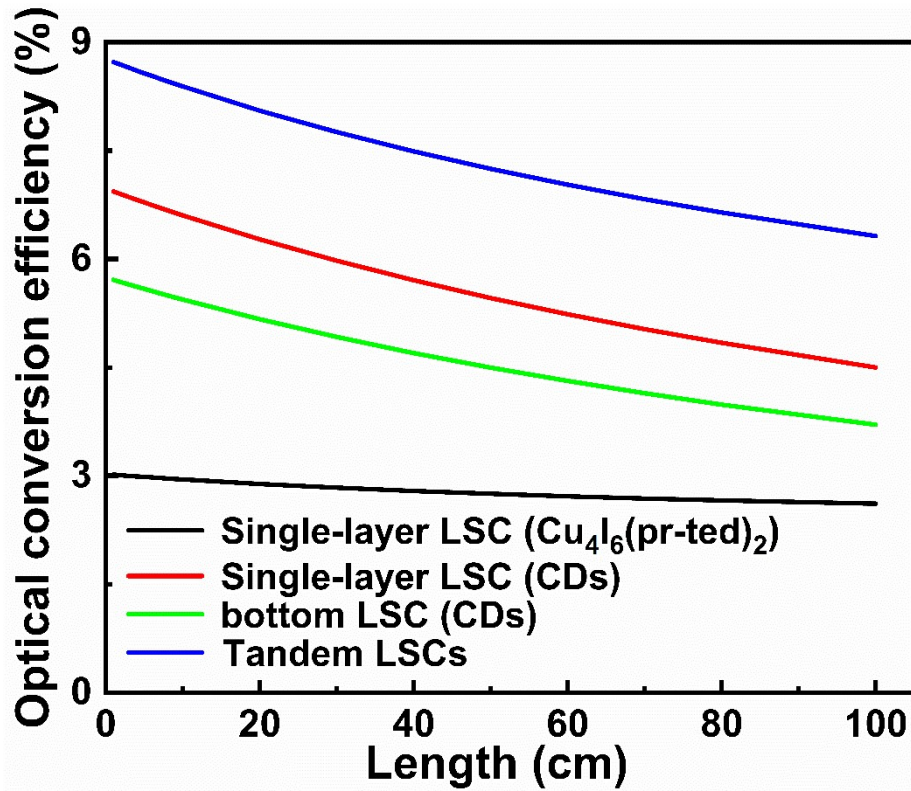
Fig. S12 Calculated the optical conversion efficiency of LSCs with different dimensions.

Table S1 Photovoltaic parameters of single and tandem LSCs.

LSC		J_{sc} (mA/cm^2)	V_{oc} (V)	FF (%)	G	η_{opt} (%)	η (%)
Single	Cu$_4$I$_6$(pr-ted)$_2$ NPs/PVP	10.35	0.50	70.41	6.25	3.60 ± 0.05	3.59 ± 0.04
Single	CDs/PMMA based LSC	8.29	0.49	68.91	6.25	2.88 ± 0.05	2.82 ± 0.04
Tandem	Cu$_4$I$_6$(pr-ted)$_2$ NPs/PVP	10.29	0.49	70.27	6.25	3.58 ± 0.06 6.40 ± 0.08	3.57 ± 0.05 6.29 ± 0.06
	CDs/PMMA based LSC	8.11	0.49	69.03	6.25	2.82 ± 0.04	2.72 ± 0.03

Table S2 The η_{opt} for the LSCs based on different luminophores, types and dimensions.

LSC	Type	η_{opt} (%)	LSC area (cm^2)	Ref.
Cu_4I_6(pr-ted)$_2$ NPs	Single	3.60	5×5	This work
CDs	Single	2.88	5×5	This work
Cu_4I_6(pr-ted)$_2$ NPs and CDs	Tandem: two layers	6.40	5×5	This work
CDs	Tandem: three layers	4.03	5×5	6
CDs	Tandem: three layers	2.3	8×8	7
CDs	Tandem: two layers	4.3	10×10	8
CDs and AIE molecules	Tandem: two layers	3.55	6.5×6.5	9
CdSe/CdS QDs and CDs	Tandem: two layers	1.4	10×10	10
perovskite QDs and CDs	Tandem: three layers	3.05	10×10	11
CDs	Single	4.74	2×2	12
0D Cs_4PbBr_6 NCs	Single	2.4	10×10	13
Copper-doped InP/ZnSe QDs	Single	3.4	10×10	14
silicone-carbon dots	Single	7.58	2.5×2.5	15
$AgInS_2$/ZnS QDs	Single	3.8	10.4×10.4	16
CdSe/CdS core/shell QDs	sandwich structure	2.95	10×10	17
mScarlet fluorescent proteins	Single	2.58	2.5×2.5	18
$CsPbI_3$ NCs	Single	3.1	2×2	19
perylene diimide-based donor–emitter fluorophore pair	Single	2.07	20×20	20

References for SI

1. W. Liu, K. Zhu, S. J. Teat, G. Dey, Z. Shen, L. Wang, D. M. O'Carroll and J. Li, *J. Am. Chem. Soc.*, 2017, **139**, 9281-9290.
2. J. J. Wang, C. Chen, W. G. Chen, J. S. Yao, J. N. Yang, K. H. Wang, Y. C. Yin, M. M. Yao, L. Z. Feng, C. Ma, F. J. Fan and H. B. Yao, *J. Am. Chem. Soc.*, 2020, **142**, 3686-3690.
3. Y. Liu, D. Chao, L. Zhou, Y. Li, R. Deng and H. Zhang, *Carbon*, 2018, **135**, 253-259.
4. Y. Liu, J. Wei, X. Yan, M. Zhao, C. Guo and Q. Xu, *Chin. Chem. Lett.*, 2021, **32**, 861-865.
5. V. I. Klimov, T. A. Baker, J. Lim, K. A. Velizhanin and H. McDaniel, *ACS Photonics*, 2016, **3**, 1138-1148.

6. J. Wang, J. Wang, Y. Xu, J. Jin, W. Xiao, D. Tan, J. Li, T. Mei, L. Xue and X. Wang, *ACS Appl. Energy Mater.*, 2020, **3**, 12230-12237.

7. L. ZdraZil, S. Kalytchuk, K. Hola, M. Petr, O. Zmeskal, S. Kment, A. L. Rogach and R. Zboril, *Nanoscale*, 2020, **12**, 6664-6672.

8. J. Li, H. Zhao, X. Zhao and X. Gong, *Nanoscale*, 2021, **13**, 9561-9569.

9. W. Ma, W. Li, R. Liu, M. Cao, X. Zhao and X. Gong, *Chem. Commun.*, 2019, **55**, 7486-7489.

10. G. Liu, H. Zhao, F. Diao, Z. Ling and Y. Wang, *J. Mater. Chem. C*, 2018, **6**, 10059-10066.

11. H. Zhao, D. Benetti, X. Tong, H. Zhang, Y. Zhou, G. Liu, D. Ma, S. Sun, Z. M. Wang, Y. Wang and F. Rosei, *Nano Energy*, 2018, **50**, 756-765.

12. Y. Li, P. Miao, W. Zhou, X. Gong and X. Zhao, *J. Mater. Chem. A*, 2017, **5**, 21452-21459.

13. H. Zhao, R. Sun, Z. Wang, K. Fu, X. Hu and Y. Zhang, *Adv. Funct. Mater.*, 2019, **29**, 1902262.

14. S. Sadeghi, H. Bahmani Jalali, S. B. Srivastava, R. Melikov, I. Baylam, A. Sennaroglu and S. Nizamoglu, *iScience*, 2020, **23**, 101272.

15. J. Wu, W. Xin, Y. Wu, Y. Zhan, J. Li, J. Wang, S. Huang and X. Wang, *Chem. Eng. J.*, 2021, **422**, 130158.

16. L. Dhamo, F. Carulli, P. Nickl, K. D. Wegner, V. D. Hodoroaba, C. Würth, S. Brovelli and U. Resch-Genger, *Adv. Opt. Mater.*, 2021, **9**, 2100587.

17. G. Liu, R. Mazzaro, Y. Wang, H. Zhao and A. Vomiero, *Nano Energy*, 2019, **60**, 119-126.

18. S. Sadeghi, R. Melikov, H. Bahmani Jalali, O. Karatum, S. B. Srivastava, D. Conkar, E. N. Firat-Karalar and S. Nizamoglu, *ACS Appl. Mater. Interfaces*, 2019, **11**, 8710-8716.

19. J. Wu, J. Tong, Y. Gao, A. Wang, T. Zhang, H. Tan, S. Nie and Z. Deng, *Angew. Chem. Int. Ed.*, 2020, **59**, 7738-7742.

20. B. Zhang, P. Zhao, L. J. Wilson, J. Subbiah, H. Yang, P. Mulvaney, D. J. Jones, K. P. Ghiggino and W. W. H. Wong, *ACS Energy Lett.*, 2019, **4**, 1839-1844.